

On Rapidly Rotating Magnetic Core-Collapse Supernovae

J. R. Wilson^{1,2}, G. J. Mathews² and H. E. Dalhed¹

¹University of California,
Lawrence Livermore National Laboratory
Livermore, CA, 94550

²Center for Astrophysics, University of Notre Dame,
Notre Dame, IN 46556, U.S.A.

ABSTRACT

We have analyzed the magnetic effects that may occur in rapidly rotating core collapse supernovae. We consider effects from both magnetic turbulence and the formation of magnetic bubbles. For magnetic turbulence we have made a perturbative analysis for our spherically symmetric core-collapse supernova model that incorporates the build up of magnetic field energy in the matter accreting onto the proto-neutron star shortly after collapse and bounce. This significantly modifies the pressure profile and increases the heating of the material above the proto-neutron star resulting in an explosion even in rotating stars that would not explode otherwise. Regarding magnetic bubbles we show that a model with an initial uniform magnetic field ($\sim 10^8$) G and uniform angular velocity of ~ 0.1 rad s⁻¹ can form magnetic bubbles due to the very non homologous nature of the collapse. It is estimated that the buoyancy of the bubbles causes matter in the proto-neutron star to rise, carrying neutrino-rich material to the neutron-star surface. This increases the neutrino luminosity sufficiently at early times to achieve a successful neutrino-driven explosion. Both magnetic mechanisms thus provide new means for initiating a Type II core-collapse supernova.

Subject headings: Gravitation - Hydrodynamics - Instabilities - Stars: rotation - Supernovae: general

1. Introduction

In most supernova models with pure spherical symmetry, after a massive star collapses due to the exhaustion of its nuclear fuel, the neutrino luminosity from the proto-neutron star (PNS) is too low to heat the in-falling material sufficiently to expel matter from the star (e.g. Bruenn 1985; 1993, Burrows, Hayes, & Fryxell 1995; Yamada et al. 1999; Fryer & Heger 2000; Rampp & Janka 2000, 2002; Liebendörfer et al. 2001; Mezzacappa et al 2001; Akiyama et al. 2003 Buras et al. 2003; Thompson, Burrows, & Pinto 2003; Burrows 2004; Cardall 2004). However, the Livermore supernova model (cf. Wilson & Mayle 1988; 1993; Wilson & Mathews 2003) avoids this problem and is able to explode in spherical symmetry by inducing a larger amount of neutrino heating soon after the core bounce. For this reason it is important to examine any possible means to induce additional heating above the proto-neutron star.

One important mechanism for such heating, for example, is that the proto-neutron star can become hydrodynamically unstable a few hundred milliseconds after the core bounce due to the so-called neutron-finger instability (Wilson & Mayle 1988; Wilson & Mathews 2003). This instability results from the build up of dense material with a large neutron-to-proton ratio near the surface of the proto-neutron star. Sufficiently neutron-rich material can overcome the buoyancy caused by the high entropy near the surface. As surface material sinks downward neutrino-rich material rises to the surface. This enhances the neutrino luminosity and produces enough heating of material behind the shock to produce an explosion (cf. Wilson & Mathews 2003).

The fact that other models of Type II supernovae do not exhibit this instability can be attributed to a number of possibilities (e.g. Bruenn et al. 2004) such as differences in the equation of state employed, the detailed way in which convection is treated, and/or the treatment of neutrino flow. Hence, this mechanism is controversial (Bruenn et al. 2004) as a means to induce core-collapse supernovae. Therefore, in this paper we describe first schematic calculations of some plausible, and perhaps more compelling, alternatives to the neutron-finger instability to overcome the lack of sufficient neutrino luminosity at early times in the explosion. We have investigated two magneto-hydrodynamic (MHD) effects both above and below the rotating proto-star surface that may be strong

enough to enhance the neutrino luminosity and produce an explosion. These processes could either increase the neutron-finger instability or replace it in models that have no surface convection.

2. Models

The purpose of the present paper is to make a schematic study of the possible roles of magneto-hydrodynamics in rotating core-collapse supernovae. While the models we utilize are adequate to illustrate the order of magnitude of these effects, we emphasize that it will be necessary to do this calculation in two or three spatial dimensional magneto-hydrodynamics (MHD) to prove that the ideas presented here are correct. Such calculations, however, present an exceedingly difficult computational challenge. For the purposes of the present schematic investigation, however, a much simpler model is employed which involves the average spherical effects of the inherently multidimensional rotation and magnetic effects as a perturbation on one-dimensional hydrodynamics. This is a reasonable approximation as a means of exploring the parameter space and extracting the essential physics as long as we are considering moderate rotation rates and relatively weak but realistic magnetic fields.

As we shall see, the main effects in our perturbation analysis are build up of magnetic turbulence and field energy above the proto-neutron star shortly after collapse and bounce due to the accretion of magnetized matter, and the formation of magnetic bubbles and magnetic-driven convection below the surface of the PNS. We demonstrate that both of these effects can significantly impact the explosion mechanism.

2.1. Supernova Model

Details of the current version of the Livermore supernova model have been described in Wilson & Mathews (2003). For completeness we here summarize the basic physics and the way in which the effects of rotation and MHD are implemented. To begin with the metric for a spherical neutron star is written in Lagrangian coordinates,

$$ds^2 = -a^2 \left[1 - \left(\frac{U}{\Gamma} \right)^2 \right] dt^2 - \frac{2aU}{\Gamma^2} dr dt + \frac{dr^2}{\Gamma^2} + r^2 (d\theta^2 + \sin^2 \theta d\phi^2) , \quad (1)$$

where a is the inverse of the time component of four velocity $a \equiv 1/U^t$. It is, thus, related to the gravita-

tional red shift. The quantity r is a distance coordinate with proper distance is given by

$$\text{Proper Distance} = \int \frac{dr}{\Gamma} . \quad (2)$$

where,

$$\Gamma \equiv \left(1 + U^2 - \frac{2M}{r} \right)^{1/2} . \quad (3)$$

The quantity M is the gravitational mass interior to r as defined below, and $U^2 = U^r U_r$ is the square of the radial component of the four velocity.

For the metric coefficient a the vanishing of the covariant derivative $T^{j\mu}_{;\mu} = 0$ implies,

$$a = \exp \left[\int_m^{m_{max}} \frac{dm}{\rho h} \left(\frac{\partial P_{eff}}{\partial m} + \frac{br^2 \rho}{a} \frac{\partial}{\partial t} \left\{ \frac{\Phi_\nu}{r^2 \rho^2} \right\} - \frac{2b\Gamma}{r} W_\nu \right) \right] , \quad (4)$$

where m_{max} is the mass coordinate at the boundary of the numerical grid. The quantity $h \equiv 1 + \epsilon + P/\rho$ is the relativistic enthalpy, and

$$b \equiv \frac{1}{4\pi r^2 \rho} . \quad (5)$$

The quantities Φ_ν and W_ν refer to the angle integrated neutrino flux and a nonthermal neutrino pressure correction factor, respectively, as described in Wilson & Mathews (2003).

2.2. Matter Equations

For the present application we write the radial four acceleration as,

$$\frac{1}{a} \frac{\partial U}{\partial t} = -\frac{\Gamma}{\rho h} \left[\frac{1}{b} \frac{\partial P_{eff}}{\partial m} + \frac{r^2 \rho^2}{a} \frac{\partial}{\partial t} \left\{ \frac{\Phi_\nu}{r^2 \rho^2} \right\} - \frac{2\Gamma}{r} W_\nu \right] - \frac{M}{r^2} - 4\pi r P_{eff} . \quad (6)$$

As discussed below, effects of rotation and magnetic field energy are absorbed into an effective pressure in the acceleration equation, i.e. we write:

$$P_{eff} = P_M + P_\nu + P_{rot} + P_{mag} , \quad (7)$$

where P_M and P_ν are the usual contributions from matter in thermal equilibrium and neutrinos which are nonthermal and must be transported explicitly. The effective pressure perturbations from rotation

and magnetic field energy, P_{rot} and P_{mag} , are defined below in section 2.5.

The condition of baryon number conservation leads to auxiliary equations for the matter evolution:

$$\rho = \frac{1}{b} \frac{\partial r}{\partial m} . \quad (8)$$

$$\frac{1}{a} \frac{\partial \rho}{\partial t} = -\rho \frac{1}{r^2} \frac{\partial}{\partial r} (r^2 U) + \frac{1}{2\Gamma} \rho r \Phi_\nu . \quad (9)$$

The gravitational mass is given by

$$M = 4\pi \int_0^m dm \frac{\partial r}{\partial m} r^2 \left[\rho(1 + \epsilon) + \frac{U}{\Gamma} \Phi_\nu \right] , \quad (10)$$

with

$$\frac{1}{a} \frac{\partial M}{\partial t} = 4\pi r^2 (UP + \Gamma \Phi_\nu) , \quad (11)$$

and

$$\frac{1}{b} \frac{\partial M}{\partial m} = 4\pi r^2 \left[\Gamma \rho(1 + \epsilon) + U \Phi_\nu \right] . \quad (12)$$

The baryon rest mass of the star is then simply given by the integral over the proper volume, $d(Vol) = 4\pi r^2 dr/\Gamma$,

$$M_0 = 4\pi \int r^2 dr \frac{\rho}{\Gamma} . \quad (13)$$

The matter internal energy evolves according to

$$\frac{1}{a} \frac{\partial \epsilon_M}{\partial t} = -P_M \frac{1}{a} \frac{\partial}{\partial t} \left(\frac{1}{\rho} \right) - \frac{1}{\rho} \sum_{i=1}^6 \int \Lambda_i dE d\Omega_\nu , \quad (14)$$

where P_M is the matter pressure and the Λ_i are various neutrino scattering and absorption source terms (Wilson & Mathews 2003). The neutrino transport is treated with appropriate flux-limited diffusion.

The condition of lepton number conservation leads to an expression for the change in the average electron fraction (or charge per baryon) Y_e due to weak interactions,

$$\frac{\rho}{m_b} \frac{1}{a} \frac{\partial Y_e}{\partial t} = - \sum_i (\Lambda_i - \bar{\Lambda}_i) \frac{dq}{q} d\Omega_\nu , \quad (15)$$

where $q \equiv a\epsilon_\nu$, ϵ_ν is the neutrino energy, and q is the energy a neutrino would have if it was removed to infinity.

2.3. Magnetic Fields

Magnetic fields are easily added to the simulation via the electromagnetic stress-energy tensor,

$$T_{\mu\nu} = T_{\mu\nu}^{\text{Fluid}} + T_{\mu\nu}^{EM} \quad , \quad (16)$$

where,

$$T_{\mu\nu}^{EM} = \frac{1}{4\pi} (g_{\alpha\mu} F^{\alpha\beta} F_{\beta\nu} - \frac{g_{\mu\nu}}{4} F^{\alpha\beta} F_{\alpha\beta}) \quad , \quad (17)$$

and as usual, the electromagnetic tensor $F_{\mu\nu}$ can be related to a vector potential A_ν ,

$$F_{\mu\nu} = \frac{\partial A_\nu}{\partial x^\mu} - \frac{\partial A_\mu}{\partial x^\nu} \quad . \quad (18)$$

In cylindrical symmetry the non-vanishing spatial components of $F_{\mu\nu}$ are thus,

$$F_{rz} = H_\phi \quad , \quad F_{r\phi} = \frac{\partial A_\phi}{\partial r} \quad , \quad F_{z\phi} = \frac{\partial A_\phi}{\partial z} \quad . \quad (19)$$

Then, from the assumption of perfect conductivity, $U^\mu F_{\mu\nu} = 0$, the space-time components can be obtained.

$$F_{tr} = V^z H_\phi + V^\phi F_{r\phi} \quad (20)$$

$$F_{tz} = V^\phi F_{z\phi} - V^r H_\phi \quad (21)$$

$$F_{t\phi} = -V^r F_{r\phi} - V^z F_{z\phi} = \frac{\partial A_\phi}{\partial t} \quad (22)$$

The time evolution of H_ϕ then can be deduced from Maxwell's equation

$$F_{rz;t} + F_{tr;z} + F_{zt;r} = 0 \quad , \quad (23)$$

which gives,

$$\frac{\partial H_\phi}{\partial t} = \frac{\partial}{\partial z} \left(V^\phi \frac{\partial A_\phi}{\partial r} \right) - V^z H_\phi - \frac{\partial}{\partial r} \left(V^\phi \frac{\partial A_\phi}{\partial z} \right) + V^r H_\phi \quad . \quad (24)$$

In the present work we ignore the back reaction of the magnetic fields on the matter fluid in the simulations, but estimate their effects below in Section 3.

2.4. Initial Conditions

To evolve the matter equations of motion 6-15, we adopt 250 nonuniform radial zones. The grid extends to ~ 170 zones above the photosphere. For the magnetic evolution we adopt 30 angular zones in a 90° quadrant so that the size of each angular zone is 3° . In our calculations the region of magnetic-driven turbulence extends over a region of $\sim 10 - 20$ radial

zones. This resolution has been employed and tested in previous supernova collapse and rotating star calculations (Wilson & Mathews 2003) and should be adequate for the analysis here.

The initial MHD model assumes that the star is rotating with a uniform angular velocity in the inner $5 M_\odot$ of the star. It is also threaded by a uniform magnetic field in the direction of the axis of rotation before the start of the dynamic core-collapse phase. Various initial models have been explored. For most of the models reported on here, the strength of the initial magnetic field is chosen such that the final neutron star would have a surface magnetic field of $H \sim 10^{12}$ G.

The initial rotational velocity in some models leads to a post collapse rotation period ($P \sim 1.4$ ms). This is close to the shortest possible Keplerian neutron-star rotation period ($P \lesssim 1$ ms, Burgio, Schulze & Weber 2003), and is comparable to the minimum values in the observed period distribution for pulsars (Phinney & Kulkarni 1994; Weber 1999; Manchester 2004). Observed young pulsars (Manchester 2004) in supernova remnants have much longer periods (~ 1 s) than that obtained in these calculations. However they also have large spin down rates. Indeed, the stars modeled here should also have a large spin-down rate. Since the poloidal field threads the rapidly rotating neutron star, and we use a massive outer envelope of very low angular velocity, a very high torque should develop between the spinning neutron star and the outer star plus magnetic field. These torques are sufficient to slow the neutron star down to well within the observed range by the time it becomes an observable pulsar.

2.5. Magnetic Turbulence above the PNS

Above the proto-neutron star for a few tenths of a second after bounce is a region below the bounce shock front and above the almost static proto-neutron star radius where matter is slowly accreting. At post bounce times typically $t_{pb} \sim 200$ ms, the proto-neutron star radius is ~ 40 km and the shock radius is ~ 170 km. Later, at $t_{pb} \approx 300$ ms, the proto-neutron star radius is 32 km and the shock radius has contracted to 140 km. The Mach number in the sub-shock region is < 0.1 .

In the sub-shock region magnetic field generation is possible for a rapidly rotating magnetized collapsing star. To model the evolution of the magnetic field,

we follow the general principles given in Balbus and Hawley (1998) [hereafter BH98].

The work of BH98 has led us to examine the stability of the accretion flow of matter in the waist region shortly after core bounce. After bounce a shock moves out above the proto-neutron star. This produces a region of slowly moving (Mach number < 0.1) matter (see Figure 1). For an initially uniformly rotating iron core this subshock region has an angular velocity profile of $\omega \propto r^{-1.8}$. While this velocity profile is different from the Keplerian profile ($\omega \propto r^{-3/2}$) studied in BH98, it is still unstable to magnetohydrodynamic flow. BH98 give a maximum growth rate of $\lambda = (r/2)(d\omega/dr) \approx 0.9\omega$. We adopt this growth rate. Hence we write: $\dot{H} = \lambda H$,

BH98 treat accretion disks that are almost static and orbital velocities that are close to Keplerian. However, in our supernova model the accretion is rapid and the angular velocity is not Keplerian.

We assume that the turbulent magnetic field amplitude then grows as

$$\tilde{H}(t) = H_0(r)e^I, \quad (25)$$

where I is the integrated growth rate

$$I = \int \lambda dt = 0.9 \int \omega dt = 0.9 \int_r^{r_{sh}} \left| \frac{\omega}{v} \right| dr, \quad (26)$$

where r_{sh} is the shock radius.

In the above, H_0 is the ordered H_Z , H_R , and H_Φ that arises from the spherical inflow of the magnetized matter. The transition to a turbulent magnetic field is assumed to be rapid on the problem time scale. For the lowest initial angular velocity that produced an explosion, $\omega = 0.071 \text{ s}^{-1}$, the integrated growth rate was $I \approx 30$ at a post bounce time of $t_{pb} = 0.14 \text{ s}$ and increased to $I \approx 90$ by $t_{pb} = 0.25 \text{ s}$.

The initial field was selected so that the final neutron star field will be $\approx 10^{12}$ Gauss. The ordered field is thus take to be $H_0 = 10^{12}(10 \text{ km}/r)^2$ Gauss. As demonstrated in BH98, the field is assumed to grow until near equipartition,

$$\frac{H_{max}^2}{8\pi\rho} \equiv \frac{\omega^2 r^2}{4}. \quad (27)$$

Energy is deposited in matter after the field surpasses the H_{max} . Hence, after $\tilde{H} = H_{max}$ we let,

$$\dot{\epsilon}_{matter} = 2\omega H_{max}^2 / 8\pi\rho. \quad (28)$$

The thermal matter pressure $P_M(\epsilon, \rho)$ above the PNS is thus augmented by Eq. 28 through the increase in ϵ_{matter} .

In addition, however, there are contributions from rotation and magnetic effects. In cylindrical coordinates the rotational energy density is just

$$E_{rot} = \frac{1}{2}\rho\omega^2 R^2. \quad (29)$$

We note that $r = R \sin(\theta)$ and deduce an effective isotropic pressure due to rotational energy from an angular average of the rotational energy,

$$P_{rot} = \frac{E_{rot}}{3} = \frac{1}{6}\rho\omega^2 r^2. \quad (30)$$

Similarly, the energy density due to the isotropic turbulent magnetic field \tilde{H} is

$$\tilde{E}_{mag} = \frac{\tilde{H}^2}{8\pi}, \quad (31)$$

The average pressure is then a third of this as is usual for an isotropic massless field. However, we then reduce this by another factor of two due to the solid angle of the directional flow of the accreting material. Hence we write

$$P_{rot} = \frac{\tilde{H}^2}{48\pi}. \quad (32)$$

Calculations were made with different initial angular velocities to find out how much rotation was needed to result in an explosion. These conditions are summarized in Table 1.

Figure 1 illustrates the effects on a rotating collapse simulation with and without effects of the magnetic turbulent pressure contribution. For this example, the rejuvenation of the shock due to magnetic field amplification above the PNS is clearly demonstrated.

2.6. Magnetic Bubble Driven Explosion below the PNS Surface

The nonhomologous collapse of a uniformly rotating iron core leads to differential rotation and the build up of a toroidal magnetic field (see Wheeler, Meier & Wilson 2002 for a general discussion and references). The toroidal field builds up to large values and produces a region unstable to magnetic buoyancy and tension as we now describe.

TABLE 1
EXPLOSION TIMES AND ANGULAR VELOCITIES

ω_0 (s^{-1})	t_{pb} ms
0.20	200
0.10	250
0.0707	340
0.05	∞

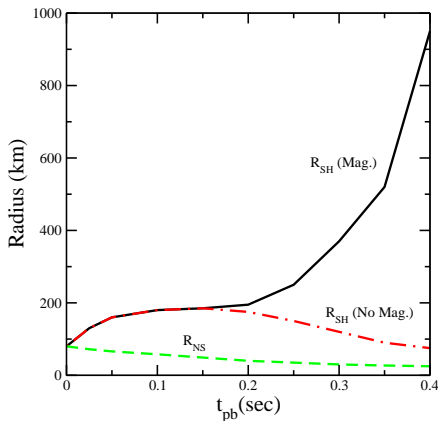


Fig. 1.— The lowest curve shows the radius of the proto-neutron star as a function of time post bounce. The upper curves give the radius of the accretion shock for models with an initial angular velocity of $\omega = 0.071 s^{-1}$ with and without magnetic turbulence as labeled. The upper curve clearly shows the effects of magnetic field amplification on the shock front. The lower curve shows that rotation alone has little effect for this particular model.

The magnetic bubble model assumes that the magnetic fields evolve in matter which can be treated as having perfect conductivity. Also, the magnetic braking back reaction of the field on the fluid is not explicitly included, though we estimate its effect. We start with the $18 M_{\odot}$ stellar progenitor model of Woosley & Weaver (1985) at the time at which the iron core has just become unstable to infall. While the hydrodynamics is assumed to evolve spherically, the magnetic field is assumed to be axially symmetric and is evolved in cylindrical coordinates. In what follows, therefore, we will need to simultaneously consider quantities in both cylindrical and spherical coordinates. Hence, we use capital R , Z , Φ to distinguish cylindrical coordinates, while r , θ , and Φ are used to denote for spherical coordinates. We assign all the matter with an angular rotational velocity ω_0 about the Z axis. A uniform magnetic field in the Z direction is assumed. Each mass shell is then zoned in the θ direction for the calculation of the magnetic fields and rotational motion.

The magnetic flux in the Z direction is taken as constant in Φ for each (r, θ) zone. Each mass shell rotates rigidly and preserves its angular momentum. As described in Section 3, these assumptions lead to the following equation for the evolution of the the toroidal field.

$$\dot{H}_{\Phi} = H_Z^0 \omega_0 \left(\frac{r_0}{r} \right)^4 \sin(\theta) \cos(\theta) \left(\frac{dr_0}{dr} \frac{r}{r_0} - 1 \right) - \frac{H_{\Phi}}{r} \frac{\partial(rv)}{\partial r} . \quad (33)$$

Note, that the $\sin(\theta) \cos(\theta)$ product implies a maximum rate of field growth in a region inclined 45° from the rotation axis.

The poloidal field components then follow from flux conservation,

$$\dot{H}_Z = H_Z^0 \left(\frac{r_0}{r} \right)^2 \left(\sin^2(\theta) \frac{dr_0}{dr} \frac{r}{r_0} + \cos^2(\theta) \right). \quad (34)$$

$$\dot{H}_R = H_Z^0 \left(\frac{r_0}{r} \right)^2 \sin(\theta) \cos(\theta) \left(\frac{dr_0}{dr} \frac{r}{r_0} - 1 \right), \quad (35)$$

where r_0 is the initial radius of a mass shell and r is the shell radius at a later time. The quantity, H_Z^0 , is the initial uniform magnetic field and ω_0 is the initial angular velocity.

The initial angular rotational velocity was chosen to be large enough that a toroidal field will build up to a size such that the buoyancy will be large enough to overcome the stabilizing outward increasing entropy gradient of the matter. Such buoyancy will then cause matter to turnover by the quasi-Ledoux convection (Wilson & Mayle 1993; Wilson & Mathews 2003). This turnover then brings ν -rich material to the surface. This enhances the neutrino luminosity enough at early times to achieve a successful explosion.

3. Results

Here, we present results for a plausible model in which the initial precollapse magnetic field, H_Z , was chosen to be 3.16×10^7 G. This field magnitude was chosen because it was estimated that the resulting neutron star would have a magnetic field of the order of 10^{12} G. Several initial angular velocities were tried in order to find the minimum amount of rotation required to produce an explosion. The minimum angular velocity was found to be 0.3 rad s^{-1} for this magnetic field strength.

This angular velocity is rather high. Nevertheless preliminary axially-symmetric hydrodynamics calculations (Tipton 2004) of the collapse of a star with $\omega = 0.3 \text{ s}^{-1}$ have found only a small distortion from sphericity for the first 0.2 s after bounce, though a vortex would form unless viscosity was included.

As noted above, this angular velocity leads to a rotation rate than is comparable to the shortest observed period pulsars and is near the maximum Keplerian limit on neutron-star spin and is somewhat larger than the rotation rate observed in young pulsars (Manchester 2004). Nevertheless, massive stars are known (e.g. Penny, Sprague & Seago 2004) to have high surface rotation velocities, typically ~ 200

km s^{-1} . If these stars rotate uniformly, then unless significant angular momentum transfer occurs during collapse, they would form a neutron star near the maximum rotation rate.

We also point out, that lower spins are required if a higher initial magnetic field is adopted. For example, a calculation was made with a smaller initial rotation rate of 0.1 rad s^{-1} and a higher precollapse magnetic field of 10^8 G. The final magnetic field was correspondingly higher (3×10^{12} G). A good explosion resulted and the final neutron star period increased to a few ms. With this scaling a final field of 10^{13} G only requires an initial rotation rate of 0.03 s^{-1} . Field strengths of $\sim 10^{13}$ are comparable to that observed in a large number of pulsars (Manchester 2004), e.g. the Crab pulsar for which $H \approx 8 \times 10^{12}$ Gauss. Indeed, it is by now well established that magnetars with fields as high as 10^{15} G exists. Such stars would require only rather small rotation rates to induce a supernova.

As the inner core of the star collapses in our benchmark model, the rotation and magnetic fields cause the collapse to become very non-homologous. Density in the inner region quickly rises from $\rho \approx 4 \times 10^9$ to a bounce density of $\sim 5 \times 10^{14} \text{ g cm}^{-3}$. Above a baryonic mass cut of about $1.5 M_\odot$ the density rises very slowly. This leads to large values of r_0/r and $(dr_0/dr)(r/r_0)$. Hence, a large H_Φ field is developed according to Eq. (33). The component H_R and H_Z rise as well but not nearly as much as H_Φ . The azimuthal H_Φ component thus becomes the dominant field component in the proto-neutron star.

A key result from these simulations is that the principle field energy density, $H_\Phi^2/8\pi$, forms two concentrated toroidal shaped regions at about 45° from the rotation axis. Figure 2 compares the magnetic tension $H^2/4\pi$ with the matter pressure along a 45° radius. The buoyancy of and tension of these toroidal regions will stir the matter and induce the transport of matter and neutrinos from the core to the surface. We here endeavor to provide an estimate of the effects of this transport on the explosion.

The motion of material due to these combined effects of rotation, magnetic buoyancy and magnetic tension is exceedingly complex and would require a fully three dimensional MHD code. Nevertheless, the essential features of this magnetic convection can be deduced via a diffusion algorithm which obeys all relevant conservation laws as it transports matter, radiation, and neutrino properties. The same algorithm

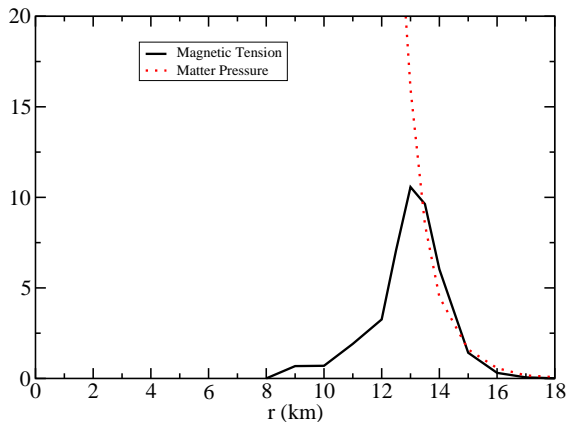


Fig. 2.— Magnetic tension (in units of $10^{30} \text{ erg cm}^{-3}$) and matter pressure (in units of $10^{31} \text{ erg cm}^{-3}$) vs radius along a line inclined at 45° to the rotation axis. Note that the magnetic field is concentrated near the neutrino-sphere which for this model is at 16.5 km. This figure represents the case of an initial magnetic field of 3.16×10^7 Gauss and a rotation rate of 0.3 rad s^{-1} at a time 0.6 s after core bounce.

as has been employed for neutron-finger convection in the Livermore supernova model (Wilson & Mathews 2003). This allows an easy comparison with results from that mechanism.

The effect of the magnetic buoyancy and tension instability is therefore modeled as follows. When the buoyancy of the magnetic field is sufficient to overcome the positive entropy gradient then a magnetic diffusion algorithm is initiated.

The problem of how the magnetic bubbles will rise and exchange energy, etc., with its surroundings is quite difficult to solve directly. To model the effect we use the existing convection algorithm in the supernova models to transport energy, composition, and neutrinos. Dimensional analysis is used to set the size of an effective diffusion coefficient, i.e. the effective diffusion coefficient is taken as scaling with the product of a mixing length times the characteristic magnetic velocity parameter.

$$D = \frac{l}{30} \sqrt{\frac{H^2}{8\pi\rho}} \quad , \quad (36)$$

where H is the maximum of the magnitude of the H_Φ field and

$$\begin{aligned} l &= r_\nu - r \quad , \quad r < r_H \\ &= r_\nu - r_H \quad , \quad r \geq r_H \quad , \end{aligned} \quad (37)$$

where r_H is the radius at which the maximum of H occurs, and r_ν is the radius of the neutrino photosphere. The factor of 30 in the denominator was deliberately assumed to be large so as to be conservative in our estimate of the size and behavior of the magnetic convective cells. A smaller cell size implies a slower convective lifetime. It should be noted that our calculation is only good enough to show the scale of rotation and magnetic field that can initiate an explosion.

As in the case of the neutron-finger instability (Wilson & Mathews 2003), the magnetic convection brings up proton-rich matter (compared to the de-leptonized surface regions) as well as neutrinos towards the surface of the proto-neutron star and results in an enhanced neutrino luminosity soon after bounce.

Figures 3-6 show some of the details of the calculation with an initial field of $3.16 \times 10^7 \text{ G}$ and a rotation rate of 0.3 rad s^{-1} . In Figures 7-9 these are compared to calculations with no convection and also those with neutron finger convection. As can be seen

in Figures 7-9, all three calculations give nearly the same behavior until a few tenths of seconds after the core bounce.

In Figure 3 the neutrino photospheric radius r_ν and the proto-neutron star average angular velocity $\bar{\omega}$ are presented. The final angular speed is very high, $\omega \approx 9 \times 10^3 \text{ rad s}^{-1}$, corresponding to a rotation period of $P \approx 1 \text{ ms}$. The star, however will quickly spin down. The surface field H_Φ is very high and it is anchored in the massive non-rotating envelope. The magnetic torque should be of order,

$$\tau_H \approx \int \left(\frac{\partial H_\Phi}{\partial R} H_Z - \frac{\partial H_\Phi}{\partial Z} H_R \right) R r^2 dr . \quad (38)$$

Putting in numbers for H_Φ , H_R , and H_Z , from the simulations, we obtain $\tau_H \approx \text{a few} \times 10^{46} \text{ erg}$. Then for a rotational moment of inertia of the nascent neutron star of $I \approx 10^{45} \text{ g cm}^2$ one has,

$$\frac{\dot{\omega}}{\omega} \approx \frac{\tau_H}{I\omega} \approx \text{a few} \times 10^{-3} \text{ s}^{-1} . \quad (39)$$

Hence the magnetic torque should be able to slow the spin of the neutron star considerably within a several minutes. The maximum values of the magnetic fields H_Z , H_Φ as a function of time are shown in Fig. 4. This figure shows that it only takes several tenths of seconds to get large magnetic fields.

Figures 5 and 6, show the radial velocity and entropy per baryon, respectively, at various times for the mass shell with the highest outward velocity in a model with magnetic convection and no neutron-finger instability. Here it is apparent from the expanding radii and increasing entropies that a good explosion has resulted. When the entropy rises to about 80 the heating by neutrino-electron scattering is equal to that of neutrino capture. Hence, even though the luminosities are falling the heating within the high-entropy bubble will remain substantial.

Figure 7 compares the electron neutrino luminosities as functions of time for three runs: no convection, neutron-finger convection, and magnetic-field driven convection. Here we see that in the case of the neutron-finger convection, luminosity comes on early but is eventually surpassed by the magnetic luminosity. The entropy profiles in radius at a time of 0.68 s post-bounce seconds are shown in Figure 8. The entropy in the magnetic case is only slightly less than of the neutron-finger case. From Fig. 9 we see that the outward velocity for the magnetic calculation is only slightly below the neutron-finger velocity.

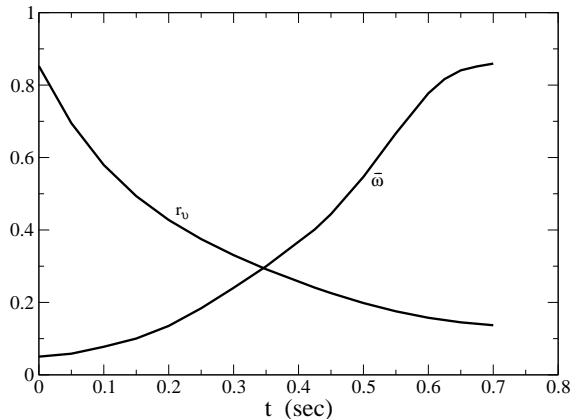


Fig. 3.— Curve marked r_ν shows the neutrino photospheric radius in units of 10^2 km versus time as the neutron star relaxes to a radius of $\sim 10 \text{ km}$. The curve labeled $\bar{\omega}$ is the angular speed (in units of 10^4 rad s^{-1}) of the proto-neutron star averaged for matter inside r_ν as a function of time.

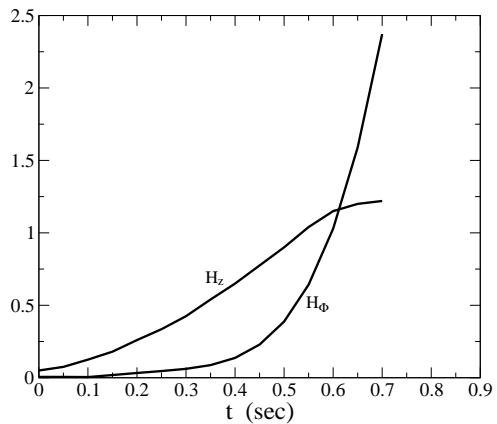


Fig. 4.— Curve H_Z shows the maximum of the Z -component of the magnetic field as a function of time in units of 10^{12} G . Curve H_Φ is the maximum value of the Φ -component of the magnetic field as a function of time in units of 10^{16} G .

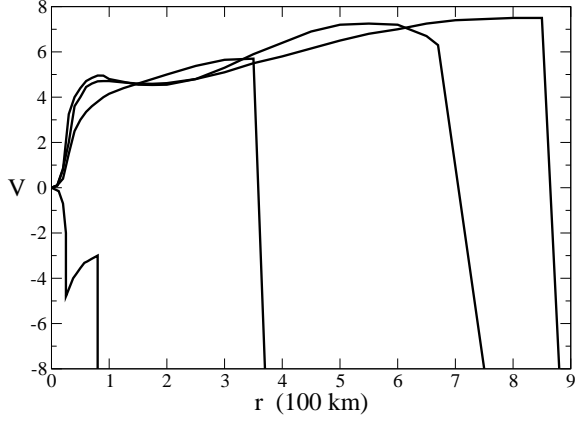


Fig. 5.— Radial velocity in units of 10^3 km s^{-1} at various indicated times post bounce (from left to right) of 0.60, 0.63, 0.66, and 0.68 s for the model with magnetic convection.

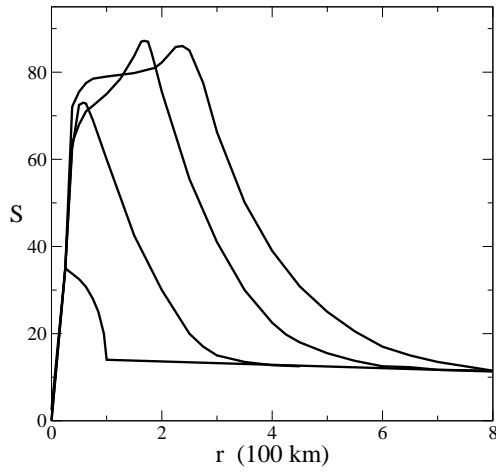


Fig. 6.— Entropy per baryon S versus radius for the post-bounce times (from left to right) of 0.60, 0.63, 0.66, and 0.68 s for the model with magnetic convection.

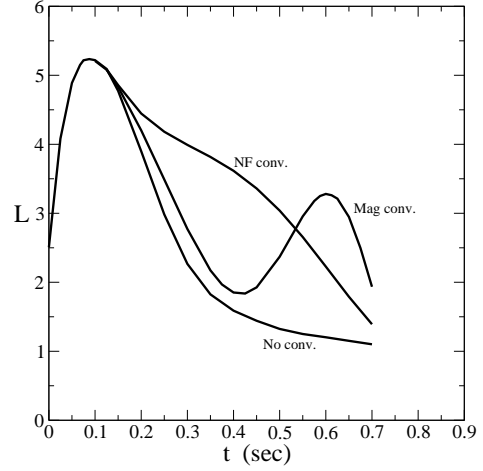


Fig. 7.— Electron neutrino luminosities in units of $10^{52} \text{ erg s}^{-1}$ as a function of post-bounce time for three calculations as labeled: no convection; neutron-finger convection, and magnetic convection. Note, that the early short-duration shock break-out luminosity has been suppressed.

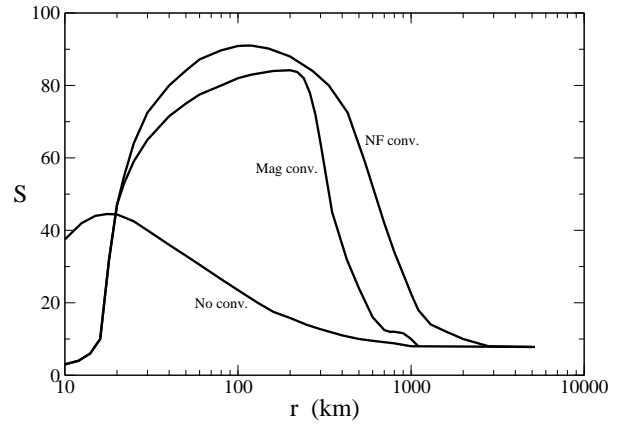


Fig. 8.— Entropy per baryon versus radius at a post-bounce time of 0.68 s for the cases of no convection; neutron-finger convection, and magnetic convection.

4. Conclusions

Although the Livermore supernova model with neutron-finger convection is a viable description of core-collapse supernovae, the present calculations suggest an alternative to the neutron-finger instability for initiating an explosion. If correct, this may provide the long sought after insight as to how core-collapse supernovae become sufficiently heated behind the shock to explode. An interesting possible side effect of the magnetic field generation that we studied is that an axial jet and/or a prolate bulge in the mass distribution should arise independently of how the convection is driven. Such features, for example, might be an explanation of the observation that most remnants emit polarized optical radiation.

It should be noted that both this magnetic turbulence effect and the magnetic bubble formation below the proto-neutron star surface will act together with neutron-fingers to induce an explosion. Clearly, more detailed work utilizing two and three dimensional MHD simulations is required to explore whether the magnetic buoyancy effect described herein is sufficient to induce an explosion. This is, however, a difficult and time-consuming calculation. It is hoped the present work will stimulate further effort to understand this possibly important contribution to the complex paradigm of core-collapse supernovae.

Work at the Lawrence Livermore National Laboratory performed in part under the auspices of the U. S. Department of Energy under contract W-7405-ENG-48 and NSF grant PHY-9401636. Work at the University of Notre Dame supported by the U.S. Department of Energy under Nuclear Theory Grant DE-FG02-95-ER40934. We acknowledge John Hawley for suggesting that we look at the effects of magnetic turbulence as a means to initiate a supernova explosion. The authors wish to thank R. Tipton of LLNL for useful discussions. They also wish to acknowledge Jonathan Wilt for help in the preparation of part of this manuscript who is also supported in part through an NSF Research Experience for Undergraduates grant at the Univ. of Notre Dame. One of the authors (JRW) also acknowledges many useful related discussions which took place at the Aspen Center for Physics.

REFERENCES

- Akiyama, S., Wheeler, J.C., Meier, D.L. & Lichtenstadt, I. 2003, ApJ, 584, 954.
- Balbus, S. A. & Hawley, J. F. 1988, Rev. Mod. Phys., 70, 1
- Bruenn, S.W. 1985, ApJ Suppl. 58, 771
- Bruenn, S. W. 1993, in Nuclear Physics in the Universe, ed. M. W. Guidry & M. R. Strayer, Proceedings of the First Symposium on Nuclear Physics in the Universe held in Oak Ridge, Tennessee, USA 24-26 September 1992 (Bristol: IOP Publishing), 31
- Bruenn, S. W., Raly, A. & Mezzacappa, A. 2004, ApJ, submitted, astro-ph/0404099
- Buras, R., Rampp, M., Janka, H. T., & Kifonidis, K. 2003, PRL, 90, 241101
- Burgio, G. F., Schulze, H.-J. & Weber, F. 2003, A&A 408, 675
- bibitemburrows Burrows, A. 2004, in *Proceedings of the Twelfth Workshop on "Nuclear Astrophysics, a Tribute to an Explosive Astrophysicist, Wolfgang Hillebrandt, on the occasion of his 60th Birthday*, Ringberg Castle, Lake Tegernsee, Germany, March 22 - 27, 2004, eds. E. Muller and H.-Th. Janka on the Physics of the r-Process, Seattle (2004) (World Scientific: Singapore) in press, astro-ph/0405427.
- Burrows, A., Hayes, J. A. & Fryxell, B. A. 1995, ApJ, 450, 830
- Cardall, C. Y. 2004, in *The r-Process: The Astrophysical Origin of the Heavy Elements and Related Rare Isotope Accelerator Physics*, Y. z. Qian, et al., Eds., (World Scientific: Singapore) pp. 186-195
- Fryer, C.L. & Heger, A. 2000, ApJ, 541, 1033
- Liebendörfer, M., Mezzacappa, A., Messer, O. E. B., Hix, R. M., Thielemann, F.-T., & Bruenn, S. W. 2001, PRD, 63, 103004
- Manchester, R. S. 2004, Science, 304 542
- Mezzacappa, A., Liebendörfer, M., Messer, O. E. B., Hix, R. M., Thielemann, F.-T., & Bruenn, S. W. 2001, Physical Review Letters, 86, 1935

Penny, L. R., Sprague, A. J. & Seago, G. 2004, ApJ, 617, 1316

Phinney, E. S. & Kulkarni, S. R. 1994, ARA&A, 32, 591

M. Rampp, M., & Janka, H.-Th. 2002, ApJL, 539, L33

M. Rampp, M., & Janka, H.-Th. 2002, A&A, 396, 361

Thompson, T.A., Burrows, A. & Pinto, P.A. 2003, ApJ, 592, 434.

Tipton, R. 2004, Priv. Comm.

Weber, F. 1999, J. Phys. G, 25, 195

Wheeler, J. C., Meier, D. L. & Wilson, J. R. 2002, ApJ, 568, 807

Wilson, J. R. & Mathews, G. J., 2003, *Relativistic Numerical Hydrodynamics*, (Cambridge University Press, Cambridge).

Wilson, J. R. & Mayle, R. W. 1988, Phys. Rep., 163, 63.

Wilson, J. R. & Mayle, R. W. 1993, Phys. Rep., 227, 97.

Woosley, S. E. & Weaver, T. A. 1995, ApJS, 101, 181

Yamada, S., Janka, H.-Th., and Suzuki, H. 1999, A&A, 344, 533

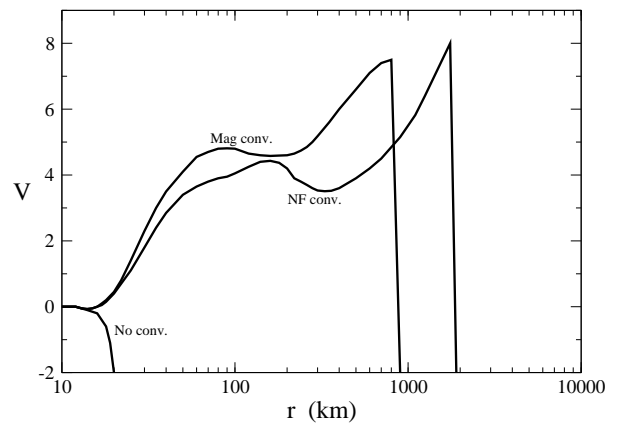


Fig. 9.— Velocity in units of 10^3 km s^{-1} at a post-bounce time of 0.68 s for the cases of no convection; neutron-finger convection, and magnetic convection.

This 2-column preprint was prepared with the AAS L^AT_EX macros v4.0.